International Journal of
Nanoscience and Nanotechnology

Research Article 2025, Volume 21, Issue 3

Fabrication and Characterization of Doped and Coupled Graphitic Carbon Nitride-Based Nanostructures with Enhanced Optical and Electronic Properties

Zahra Soleimani[1], Fariba Fathirad[1*], Mansoureh Behzadi[2]

Received 10 March 2025
Accepted 20 May 2025
Published 30 September 2025

DOI: 10.22034/ijnn.2025.2055216.2640

International Journal of Nanoscience and Nanotechnology

Abstract

In this study, graphitic carbon nitride (g-C_3N_4) nanosheets were successfully synthesized and systematically modified through nitrogen and sulfur doping, as well as heterojunction coupling with bismuth vanadate ($BiVO_4$) and manganese-doped $BiVO_4$ (Mn-$BiVO_4$), to enhance their physicochemical and optoelectronic properties. A series of nanocomposites, including S-g-C_3N_4/$BiVO_4$, N-g-C_3N_4/$BiVO_4$, S-g-C_3N_4/Mn-$BiVO_4$, and N-g-C_3N_4/Mn-$BiVO_4$ were fabricated via controlled hydrothermal and coupling strategies. Comprehensive structural and morphological characterizations were performed using field emission scanning electron microscopy (FESEM), transmission electron microscopy (TEM), energy-dispersive X-ray spectroscopy (EDX), and X-ray diffraction (XRD). The effects of doping and heterojunction formation on the optical band gap and light absorption capability were assessed using UV-Vis diffuse reflectance spectroscopy (DRS). The results confirmed that both elemental doping and heterostructure formation induced favorable modifications in the crystal structure and band alignment, thereby enhancing visible-light absorption and reducing the band gap energy. These findings demonstrate the potential of the designed nanostructures as efficient photocatalytic platforms for sustainable energy and environmental applications.

Keywords: Graphitic Carbon Nitride; Elemental Doping; Heterojunction; Optical Band Gap

How to cite this article
Soleimani Z, Fathirad F, Behzadi M. Fabrication and Characterization of Doped and Coupled Graphitic Carbon Nitride-Based Nanostructures with Enhanced Optical and Electronic Properties. Int. J. Nanosci. Nanotechnol., 2025;3: 175-179. DOI: 10.22034/ijnn.2025.2055216.2640

1. Introduction

In recent decades, the rapid increase in global energy demand and the environmental consequences of fossil fuel consumption have intensified the search for sustainable and eco-friendly energy alternatives [1-3]. Among emerging technologies, photocatalysis has garnered substantial attention due to its dual capacity to facilitate clean energy generation and environmental remediation. Prominent photocatalytic applications include CO_2 reduction, degradation of hazardous organic pollutants, and solar-driven water splitting for hydrogen production [4,5]. In photocatalytic water splitting, semiconducting materials absorb solar photons to generate electron-hole pairs, which participate in redox reactions to convert water into molecular hydrogen and oxygen [6-8]. For a semiconductor to be effective in photocatalytic processes, it must exhibit strong visible-light absorption, a suitably positioned band gap, efficient separation and migration of charge carriers, and high chemical stability in aqueous environments [9-11].

Graphitic carbon nitride (g-C_3N_4), a metal-free polymeric semiconductor with an optical band gap of approximately 2.7 eV, has emerged as a promising photocatalyst due to its high thermal and chemical stability, non-toxic nature, low cost, and facile synthesis from abundant precursors [12, 13].

However, the intrinsic drawbacks of g-C_3N_4, including limited visible-light absorption range, low surface area, and rapid recombination of photogenerated charge carriers, significantly hinder its photocatalytic efficiency [14-16].

To address these limitations, several modification strategies have been developed, such as tuning the morphology and crystallinity [17,18], constructing heterojunctions and semiconductor composites [19,20], and introducing heteroatom dopants, both metallic and non-metallic, into the g-C_3N_4 framework [21-23]. These approaches aim to narrow the band gap, enhance light-harvesting capability, improve

[1] *Department of Nanotechnology, Graduate University of Advanced Technology, Kerman, Iran.*

[2] *Department of Mining Engineering, High Education Complex of Zarand, Shahid Bahonar University of Kerman, Zarand, Iran.*

E-mail: f.fathirad7@gmail.com

charge separation dynamics, and create more catalytically active sites.

In this context, the present study focuses on the synthesis and systematic modification of g-C_3N_4 nanosheets via nitrogen and sulfur doping and coupling with $BiVO_4$ and Mn-doped $BiVO_4$ to form heterostructured nanocomposites. The aim is to investigate how these modifications influence the structural, morphological, optical, and electronic properties of the materials, thereby providing insights into the design of efficient photocatalysts for sustainable energy applications.

2. Experimental

2.1 Materials and Apparatus

All chemical reagents were of analytical grade and used without further purification. Urea (CH_4N_2O, 99.5%), sodium sulfide nonahydrate ($Na_2S{\cdot}9H_2O$, 98%), bismuth(III) nitrate pentahydrate ($Bi(NO_3)_3{\cdot}5H_2O$, 98%), ethylene glycol ($C_2H_6O_2$, 97%), manganese nitrate ($Mn(NO_3)_2$, 98%), sodium orthovanadate (Na_3VO_4, 99%), and ethanol (C_2H_5OH, 99%) were procured from Merck Co., Ltd.

The phase composition and crystallographic structure of the synthesized samples were examined using X-ray diffraction (XRD) analysis conducted on a Rigaku D-max C III diffractometer equipped with Cu Kα radiation (λ = 1.5406 Å). Additional XRD patterns were recorded using the X'Pert PRO MPD system for higher-resolution analysis.

Surface morphology and microstructural features were observed via field emission scanning electron microscopy (FESEM) using a MIRA3 TESCAN-XMU instrument, while elemental composition and distribution were analysed through energy-dispersive X-ray spectroscopy (EDX) attached to the same FESEM system.

Ultraviolet-visible diffuse reflectance spectra (UV-Vis DRS) were recorded using a Shimadzu UV-160A spectrophotometer to determine the optical properties and band gap energies. Transmission electron microscopy (TEM) imaging was performed on an FEI TECHNAI F20 microscope to investigate nanoscale structural features and interfacial characteristics of the hybrid materials.

2.2. Synthesis of Graphitic Carbon Nitride (g-C_3N_4) Nanosheets

Graphitic carbon nitride (g-C_3N_4) nanosheets were synthesized via thermal polycondensation of urea. In a typical procedure, 10 g of urea was placed in a covered ceramic crucible and thermally treated in a muffle furnace at 550 °C for 2 hours under ambient atmosphere. Upon cooling to room temperature, the resulting yellow solid was collected and finely ground using an agate mortar to obtain homogeneous g-C_3N_4 powder for subsequent modifications.

2.3. Synthesis of Nitrogen-Doped Graphitic Carbon Nitride (N-g-C_3N_4)

To introduce nitrogen dopants, 0.1 g of the as-prepared g-C_3N_4 was dispersed in 80 mL of a urea-saturated aqueous solution and stirred magnetically at 60 °C for 4 hours to ensure uniform interaction. The resulting suspension was transferred into a Teflon-lined stainless-steel autoclave and subjected to hydrothermal treatment at 150 °C for 6 hours. After cooling, the precipitate was collected, thoroughly washed with deionized water, and dried at 60 °C for further use.

2.4. Synthesis of Sulfur-Doped Graphitic Carbon Nitride (S-g-C_3N_4)

Sulfur doping was achieved by dispersing 0.32 g of g-C_3N_4 in 100 mL of an aqueous solution containing 4.8 g of sodium sulfide nonahydrate ($Na_2S{\cdot}9H_2O$). The mixture was stirred continuously at room temperature for 48 hours to facilitate sulfur incorporation. The product was then separated by centrifugation, thoroughly washed with deionized water to remove residual ions, and dried at 80 °C for 12 hours.

2.5. Synthesis of Bismuth Vanadate ($BiVO_4$) Nanosheets

To prepare $BiVO_4$, 1.1 g of $Bi(NO_3)_3{\cdot}5H_2O$ was dissolved in 30 mL of ethylene glycol (EG), followed by the addition of 0.93 g of sodium orthovanadate. The mixture was transferred into a 100 mL Teflon-lined autoclave and heated at 160 °C for 3 hours. After natural cooling to room temperature, the resulting $BiVO_4$ precipitate was collected and dispersed in deionized water. The dispersion was then subjected to ultrasonication (20 kHz, 200 W) for 30 min to exfoliate the $BiVO_4$ into thin nanosheets. Finally, the exfoliated product was washed with deionized water and ethanol, and dried at 60 °C to obtain $BiVO_4$ nanosheets [24].

2.6. Synthesis of Manganese-Doped Bismuth Vanadate (Mn-$BiVO_4$)

Mn-$BiVO_4$ was synthesized by introducing manganese as a dopant during $BiVO_4$ formation. Specifically, 0.02 g of manganese nitrate ($Mn(NO_3)_2$) was dissolved in 10 mL of distilled water and slowly added to the precursor solution of $Bi(NO_3)_3{\cdot}5H_2O$ and Na_3VO_4 in ethylene glycol under magnetic stirring for 4 hours. The mixture was then transferred into a sealed autoclave and heated at 120 °C for 36 hours. The obtained yellow residue was thoroughly washed with deionized water and ethanol, and dried at 60 °C overnight [24].

2.7. Synthesis of S-g-C_3N_4/Mn-$BiVO_4$ and N-g-C_3N_4/Mn-$BiVO_4$ Nanocomposites

To fabricate heterostructured nanocomposites, 15 mg of Mn-$BiVO_4$ was mixed separately with 15 mg of either S-g-C_3N_4 or N-g-C_3N_4 in 100 mL of a mixed solvent containing ethanol and deionized water (1:1 v/v). Each suspension was subjected to ultrasonication for 30 minutes to promote homogeneous dispersion, followed by magnetic stirring at 25 °C for 1.5 hours to ensure effective coupling. The resulting solids were separated, washed, and dried at 80 °C for 24 hours to obtain the final nanocomposites.

2.8. Synthesis of Additional Nanostructured Composites

Other g-C_3N_4-based nanocomposites were synthesized by following the same coupling protocol as described in Section 2.7. Specifically, 15 mg of each synthesized

component was dispersed in 100 mL of an ethanol/deionized water mixture (1:1 v/v), followed by ultrasonication, magnetic stirring, and drying under identical conditions to ensure consistency in material processing.

3. Results and Discussion

3.1. Characterization of the Samples

3.1.1. The Effect of Doping and Coupling on Crystalline Structure

The XRD patterns of N-g-C_3N_4/$BiVO_4$, S-g-C_3N_4/$BiVO_4$, S-g-C_3N_4/Mn-$BiVO_4$, and N-g-C_3N_4/Mn-$BiVO_4$ nanostructures are presented in Figure 1. The XRD patterns of g-C_3N_4/$BiVO_4$ and g-C_3N_4/Mn-$BiVO_4$ were previously reported in one of our research articles [24], and are reproduced here for better comparison. The characteristic peaks corresponding to $BiVO_4$ and g-C_3N_4 are observed in all samples. For g-C_3N_4-based materials, two typical peaks at around 13.1° and 27.4° are assigned to the (100) and (002) planes, respectively, where the former is attributed to the in-plane structural packing motif of tri-s-triazine units, and the latter to the interlayer stacking of conjugated aromatic systems.

In the N-g-C_3N_4/Mn-$BiVO_4$ and N-g-C_3N_4/$BiVO_4$ samples, the (100) peak slightly shifts to higher angles, indicating a possible lattice contraction due to N doping, which alters the periodic arrangement of the tri-s-triazine units. Conversely, in S-g-C_3N_4/$BiVO_4$ and S-g-C_3N_4/Mn-$BiVO_4$, the (002) peak shows a slight shift toward lower 2θ values, suggesting an expansion in interlayer distance due to S incorporation, which introduces distortion in the conjugated layers.

Moreover, in Mn-doped $BiVO_4$-based nanocomposites, including S-g-C_3N_4/Mn-$BiVO_4$ and N-g-C_3N_4/Mn-$BiVO_4$, a further shift in the XRD peaks toward higher 2θ values is evident. This shift can be attributed to the substitution of larger Bi^{3+} ions with smaller Mn^{2+} ions, leading to unit cell shrinkage due to the smaller ionic radius of Mn^{2+} compared to Bi^{3+}.

3.1.2. The Effect of Doping on Size, Morphology and Structure

In Figure 2(a,b), FESEM images of g-C_3N_4/$BiVO_4$ and S-g-C_3N_4/Mn-$BiVO_4$ nanostructures are presented. The g-C_3N_4/$BiVO_4$ sample shows a heterogeneous microstructure composed of stacked, sheet-like g-C_3N_4 layers, which appear with a darker contrast due to the presence of C and N light elements. Dispersed over these sheets are brighter, plate-like $BiVO_4$ particles with relatively small lateral dimensions and a non-uniform distribution. This contrast distinction is attributed to the higher atomic number of Bi, resulting in stronger electron backscattering.

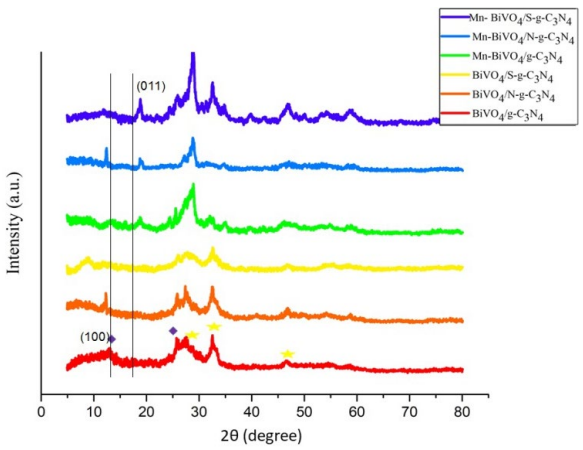

Fig. 1. XRD patterns of the synthesized nanostructures.

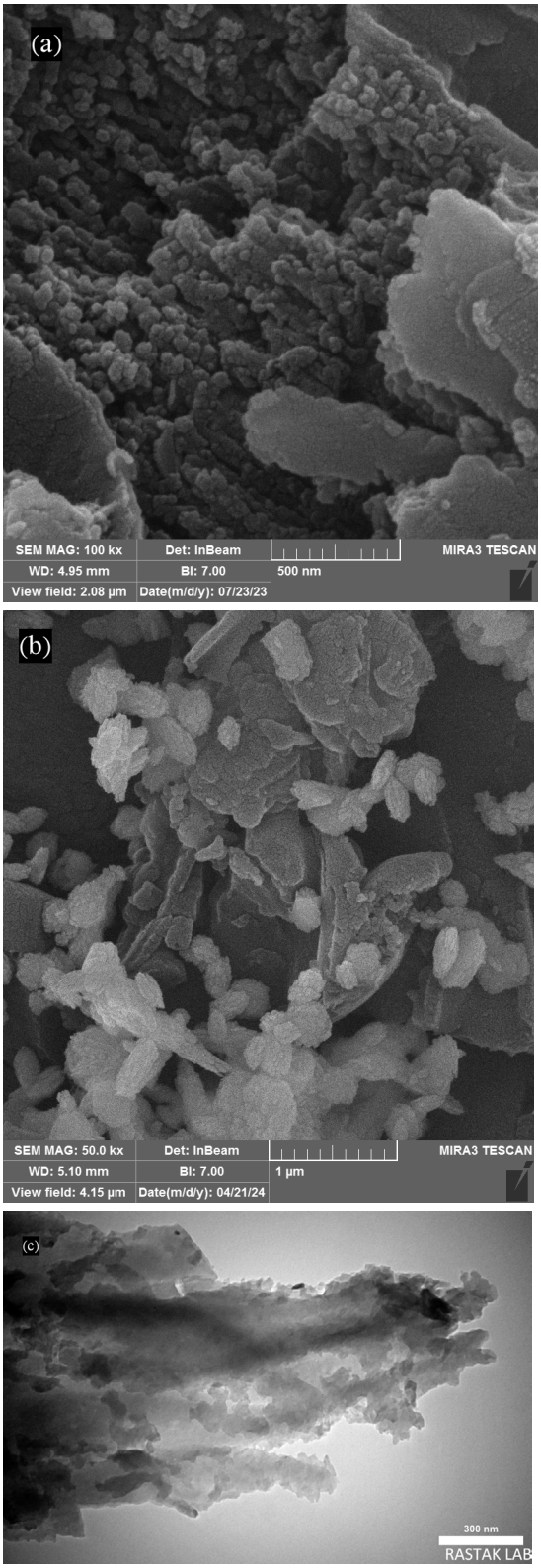

Fig. 2. FESEM images of (a) g-C_3N_4/$BiVO_4$ and (b) S-g-C_3N_4/Mn-$BiVO_4$ nanostructures; (c) TEM image of S-g-C_3N_4/Mn-$BiVO_4$ nanostructure.

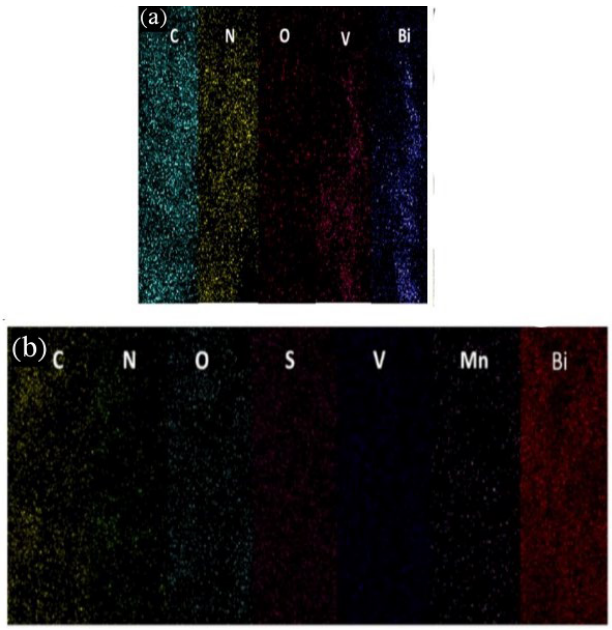

Fig. 3. EDX mapping of (a) g-C_3N_4/$BiVO_4$ and (b) Mn-$BiVO_4$/S-g-C_3N_4 nanostructures.

Upon co-doping with sulfur and manganese on the S-g-C_3N_4/Mn-$BiVO_4$ sample, the $BiVO_4$ plates become more aggregated and exhibit an increased lateral width. These morphological changes indicate improved interfacial contact, which is potentially beneficial for charge separation in photocatalytic applications. TEM images (Figure 2(c)) also confirm this claim.

3.1.3. The Effect of Doping on Elemental Distribution

EDX analyses in Figure 3(a,b) confirmed the presence of C, N, Bi, V, and O elements in g-C_3N_4/$BiVO_4$ and C, N, S, O, V, Mn, and Bi elements in the S-g-C_3N_4/Mn-$BiVO_4$ samples. According to the surface mapping, the components are dispersed uniformly in the nanohybrid.

3.1.4. The Effect of Doping on Band Gap, Optical and Electronic Properties

UV-Vis spectra were recorded to investigate the electronic properties of the samples (Figure 4a). The UV–Vis spectra of g-C_3N_4/$BiVO_4$ and g-C_3N_4/Mn-$BiVO_4$ were previously reported in our research article [24] and are reproduced here for comparison with the newly synthesized samples. The bands at around 280 and 320-500 nm is related to the π-π* transitions of the aromatic rings in g-C_3N_4 and $BiVO_4$ structures. Clearly, with increasing dopant content, the intensity of absorption increases, and a slight red shift is seen in the peaks. The maximum absorption is related to the Mn-$BiVO_4$/S-C_3N_4 sample. The band gaps of synthesized samples were estimated to be 2.0-2.75 eV by extrapolation of the tangent to the x-axis according to the $(Ahu)^2=B(hu-Eg)$ equation (Figure 4b). The highest absorption activity and the lowest band gap (Eg = 2.0 eV) were calculated for Mn-$BiVO_4$/S-C_3N_4 sample.

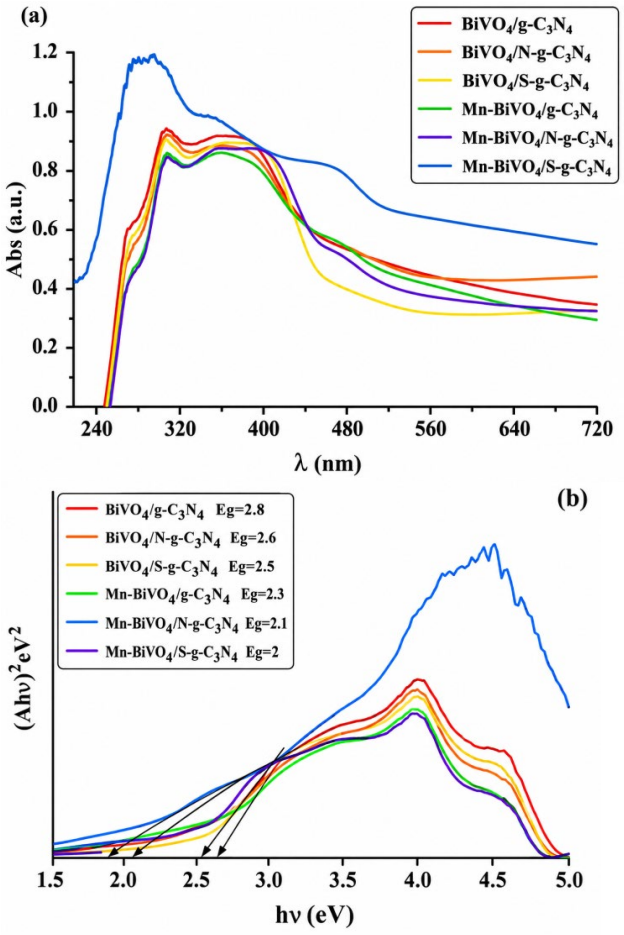

Fig. 4. (a) DRS spectra and (b) Tauc plot of the nanostructures.

4. Conclusion

In recent years, the use of semiconductor nanomaterials as photocatalysts has received wide attention in energy applications. Graphitic carbon nitride, due to its high electron-hole pair recombination rate, needs modification. Herein, sulfur and nitrogen doping and coupling with manganese- doped bismuth vanadate were performed to modify the optical and electronic structures. Various characterization techniques confirmed the successful fabrication of all nanostructures.

Based on the results obtained from the XRD, FESEM-EDX, TEM, and DRS analyses, the novel Mn-BiVO4/S-g-C3N4 nanostructure can be proposed as a promising active semiconductor among the different synthesized nanostructures.

As a result, the construction of the Mn-$BiVO_4$/S-g-C_3N_4 photocatalyst leads to high photocatalytic performance due to the modified band gap. Additional defects created by Mn and S in the structure inhibit the back-flow of electrons, thereby enhancing the charge separation efficiency.

Conflicts of interest

The authors declare that they have no conflict of interest.

Acknowledgements

The authors sincerely thank all individuals and institutions whose support and insights contributed to the completion of this work.

References

1. Etanya TF, Tsafack P, Ngwashi DK. Grid-connected distributed renewable energy generation systems: Power quality issues, and mitigation techniques - A review. Energy Rep. 2025;13:3181-3203. https://doi.org/10.1016/j.egyr.2025.02.050
2. Bendig D, Brüss L, Degen F. Entrepreneurship in the renewable energy sector: A systematic literature review of types, characteristics, and sustainability impacts. Renew Sustain Energy Rev. 2025;212:115337. https://doi.org/10.1016/j.rser.2025.115337
3. Das P. Investigation of CO2 production from agriculture and food industries, potential mitigating through solar photovoltaic pumping system and renewable energy systems: Environmental impact assessment - A review. Food Humanit. 2025;4:100523. https://doi.org/10.1016/j.foohum.2025.100523
4. Wang Q, Dong Y, Zhu J, Han J, Li Z, Xu D, et al. Critical review on emerging photocatalytic membranes for pollutant removal: From preparation to application. Talanta. 2025;287:127561. https://doi.org/10.1016/j.talanta.2025.127561
5. Du J, Ahmad I, Ashraf IM, Ahmed FBM, Aslam A, Ali I, et al. Advancements in dual S-scheme heterojunction systems for photocatalytic applications: A mini-review. Int J Hydrogen Energy. 2025;100:1361-1384. https://doi.org/10.1016/j.ijhydene.2024.12.421
6. Zainal BS, Ker PJ, Mohamed H, Ong HC, Fattah IMR, Rahman SMA, et al. Recent advancement and assessment of green hydrogen production technologies. Renew Sustain Energy Rev. 2024;189:113941. https://doi.org/10.1016/j.rser.2023.113941
7. Liao CH, Huang CW, Wu JCS. Hydrogen Production from Semiconductor-based Photocatalysis via Water Splitting. Catalysts. 2012;2(4):490-516. https://doi.org/10.3390/catal2040490
8. Jiang D, Zhao H, Jia Z, Cao J, John R. Photoelectrochemical behaviour of methanol oxidation at nanoporous TiO2 film electrodes. J Photochem Photobiol A. 2001;144(2-3):197-204. https://doi.org/10.1016/S1010-6030(01)00527-5
9. Mishra S, Rashmi A. Photocatalytic applications of graphene-based semiconductor composites: A review. Mater Today Proc. 2021;35:164-169. https://doi.org/10.1016/j.matpr.2020.04.066
10. Gholami Akerdi A, Hajir Bahrami S. Application of heterogeneous nano-semiconductors for photocatalytic advanced oxidation of organic compounds: A review. J Environ Chem Eng. 2019;7(5):103283. https://doi.org/10.1016/j.jece.2019.103283
11. Karthikeyan C, Arunachalam P, Ramachandran K, Al-Mayouf AM, Karuppuchamy S. Recent advances in semiconductor metal oxides with enhanced methods for solar photocatalytic applications. J Alloys Compd. 2020;828:154281. https://doi.org/10.1016/j.jallcom.2020.154281
12. Safaei J, Mohamed NA, Mohamad Noh MF, Soh MF, Ludin NA, Ibrahim MA, et al. Graphitic carbon nitride (g-C3N4) electrodes for energy conversion and storage: a review on photoelectrochemical water splitting, solar cells and supercapacitors. J Mater Chem A. 2018;6(45):22346-22380. https://doi.org/10.1039/C8TA08001A
13. Wang J. Development of Graphitic Carbon Nitride based Semiconductor Photocatalysts for Organic Pollutant Degradation [dissertation]. Stockholm: KTH Royal Institute of Technology; 2015.
14. Wang R, Yan J, Zu M, Yang S, Cai X, Gao Q, et al. Facile synthesis of interlocking g-C3N4/CdS photoanode for stable photoelectrochemical hydrogen production. Electrochim Acta. 2018;279:74-83. https://doi.org/10.1016/j.electacta.2018.05.076
15. Singh J, Arora A, Basu S. Synthesis of coral like WO3/g-C3N4 nanocomposites for the removal of hazardous dyes under visible light. J Alloys Compd. 2019;808:151734. https://doi.org/10.1016/j.jallcom.2019.151734
16. Mishra A, Mehta A, Basu S, Shetti NP, Reddy KR, Aminabhavi TM. Graphitic carbon nitride (g-C3N4)-based metal-free photocatalysts for water splitting: a review. Carbon. 2019;149:693-721. https://doi.org/10.1016/j.carbon.2019.04.104
17. Toie T, Fathirad F. 0D/2D CuCo2O4/Ti3C2 hybrid nanostructure as anodic nanocatalyst for direct power generation in fuel cells: Investigating annealing temperature and synergetic effect. Inorg Chem Commun. 2024;168:112877. https://doi.org/10.1016/j.inoche.2024.112877
18. Dey KK, Gahlawat S, Ingole PP. BiVO4 optimized to nano-worm morphology for enhanced activity towards photoelectrochemical water splitting. J Mater Chem A. 2019;7(37):21207-21221. https://doi.org/10.1039/C9TA07353A
19. Bera S, Lee SA, Kim CM, Khan H, Jang HW, Kwon SH. Controlled Synthesis of Vertically Aligned SnO2 Nanograss-Structured Thin Films for SnO2/BiVO4 Core-Shell Heterostructures with Highly Enhanced Photoelectrochemical Properties. Chem Mater. 2018;30(23):8501-8509. https://doi.org/10.1021/acs.chemmater.8b03179
20. Fathirad F, Samareh F, Bahador AR. 0D/1D CdSe@CdS QDs/GONRs nanocatalyst for efficient photoelectrochemical water splitting. Appl Phys A. 2023;129(1):42. https://doi.org/10.1007/s00339-022-06326-x
21. Dagar P, Kumar S, Kumar Ganguli A. Effect of Mn2+ incorporation on the photoelectrochemical properties of BiVO4. New J Chem. 2022;46(6):2875-2883. https://doi.org/10.1039/D1NJ05292F
22. Shen S, Ke T, Fang D, Lin D. N and S co-doping of TiO2@C derived from in situ oxidation of Ti3C2 MXene for efficient persulfate activation and sulfamethoxazole degradation under visible light. Sep Purif Technol. 2022;297:121460. https://doi.org/10.1016/j.seppur.2022.121460
23. Huang K, Li C, Zhang X, Wang L, Wang W, Meng X. Self-assembly synthesis of phosphorus-doped tubular g-C3N4/Ti3C2 MXene Schottky junction for boosting photocatalytic hydrogen evolution. Green Energy Environ. 2023;8(1):233-245. https://doi.org/10.1016/j.gee.2021.03.011
24. Soltaninezhad F, Fathirad F. Synthesis and characterization of g-C_3N_4/$BiVO_4$ nanosheets: Exploring the effect of doping and heterostructure coupling on photoelectrochemical performance. Diam Relat Mater. 2025;159:112760. https://doi.org/10.1016/j.diamond.2025.112760